Chapter 4

Dynamics of a 2D Vibrated Model Granular Gas in Microgravity

Yan Grasselli, Georges Bossis, Alain Meunier and Olga Volkova

Additional information is available at the end of the chapter

http://dx.doi.org/10.5772/intechopen.68277

Abstract

We are reporting an experimental study performed on a granular gas enclosed into a 2D cell submitted to controlled external vibrations. Experiments are performed in microgravity during parabolic flights. High-speed optical tracking allows to obtain the kinematics of the particles and the determination of all inelastic parameters as well as the translational and rotational velocity distributions. The energy into the medium is injected by submitting the experimental cell to an external and controlled vibration. Two model gases are studied beads and disks; the latter being used to study the rotational part of the particle's dynamics. We report that the free cooling of a granular medium can be predicted if we consider the velocity dependence of the normal restitution coefficient and that the experimental ratio of translational versus rotational temperature decreases with the density of the medium but increases with the driving velocity of the cell. These experimental results are compared with existing theories. We also introduce a model that fairly predicts the equilibrium temperatures along the direction of vibration.

Keywords: granular, microgravity, translational temperature, rotational temperature

1. Introduction

Granular gases are suspensions in air of macroscopic particles whose dynamics is ruled by momentum transfer during collisions between the particles. Unlike molecular gases, these collisions are not elastic, and the dissipation resulting of each collision gives important qualitative differences, since without bringing energy to the system, the motion of the particles will quickly stop. The supply of energy can be natural, as it is the case with gravity forces during avalanches or due to a flow of fluid through a bed of particles, or artificial for instance by shaking a box containing the grains. Due to the importance of granular flows in many industries, they have been the subject of intensive research and numerous reviews [1–5].

Gravity is, of course, a fundamental parameter, which governs the density distribution of particles with height in a sheared flow or in a vibrated container. The understanding of the complex physics of these granular systems is then complicated by the presence of the gravity. Besides, numerical simulations allow to obtain information on the dynamics of model systems of granular particles without the need to use sophisticated experiments in parabolic flights, drop tower or suborbital rocket flight but can't replace real experiments [6–9].

Two specific phenomena of the dynamics of a vibrated granular are the clustering instabilities, which occur due to the dissipation in multiple collisions between grains and the violation of the equipartition energy between each translational and rotational degree of freedom.

Recent results, obtained by molecular dynamics simulations of a box with two opposite vibrating walls and fixed side walls, have shown that in zero gravity the cluster of particles oscillate around its equilibrium position [10]. Experiments made in a parabolic flight in similar conditions with two opposite vibrating walls and with two different sizes of particles (diameter of 1 and 2 mm) were compared to simulation results. A phase diagram of clustering versus the volume fraction of each species obtained by numerical simulation was well agreeing with the experimental results and showed a segregation effect [11]. A different kind of cluster consisting of regular alignments of particles along the velocity lines in a Couette flow was also found in parabolic flight experiments [12].

Concerning the temperature of a vibrated granular gas, it was shown to follow a power law: $T = CV_p^{\alpha}$, where V_p is the peak amplitude of the vibration velocity and $1 < \alpha < 2$. In a recent paper [13], it was demonstrated that the different values of the power α were related to the ratio, W, of the energy injected by the vibration mV_p^2 to the gravitational potential energy. When W is large, that is, to say when the gravity is negligible, the value $\alpha = 2$ is recovered. A balance of the energy flux injected by the vibrated wall with the dissipation induced by particle-particle and particle-wall collisions allows to demonstrate that the temperature along the direction of vibration should be larger than the transverse temperature and that this ratio increases when the radial restitution coefficient decreases [43]. It was also found theoretically [38] that, even if the temperature of translational and rotational degrees of freedom were initially identical, the decrease of the translational temperature, after switching off the energy supply, was much faster than the rotational one but both of them are predicted to have a decrease in t^{-2} as predicted by Haff's law, although at longer time, the system becomes inhomogeneous and follows a decrease with $t^{-6/5}$ [14]. The t^{-2} decrease and the difference between translational and rotational energies were also obtained by numerical simulations for particles with a needle shape [15]. In simulations of the cooling of a gas of ellipsoidal grains with different aspect ratio [16], the authors have also found a t^{-2} law in all cases, but when the aspect ratio (a/b) increases the difference between the translational and rotational temperature decreases and had totally disappeared for a/b = 2, even becoming slightly larger than one for larger values of a/b. This is explained by the fact that the coupling between translational and rotational velocity is strongly increased by the shape's anisotropy. Also, they do not observe significant deviation from the Gaussian distribution for the velocity distribution. On the other hand, experiments in a rocket flight with a box having three moveable walls and containing needles of aspect ratio close to 10 [17] show a non-Gaussian distribution of the velocities in the excitation direction. In this experiment, the temperature perpendicular to the excitation

direction as well as the rotational temperature was approximately two times less than the temperature in the excitation direction. In this last experiment, the positions of the particles were determined with the help of two video cameras at right angle, and the determination of the positions and orientations was done manually from each video frame. Although the physics of 2D and 3D system can differ in some aspects, the use of cells where particles are confined in 2D allows a much easier tracking of the particles and an automatic detection of their position. Such experiments made in low gravity with a determination of the trajectories of each particle are scarce but very useful to check the validity of models and of numerical simulations. This is the case for instance with the confirmation of the difference of the temperatures in the directions parallel and perpendicular to the external vibration [18] and for the comparison of the cooling time with the theoretical expression [19] where the experiment gave a time of the same order of magnitude as the theory: $\tau_{exp} = 38\ ms$ against $\tau_{th} = 60\ ms$ [20].

Two model systems made of inelastic hard spheres or disks will be used as reference models to study the dynamics. The general experimental situation is to have the particles enclosed in a vibrated box (for energy input) where the vibration parameters (amplitude and frequency) are monitored. Direct optical observations can lead to the dynamics of individual particle and to retrieve the physical data. The collisions between particles are leading the dynamics of the system through the inelastic interactions and momentum transfer. The normal and tangential restitution coefficients depend on the material of the particles but sometimes also on the impact velocity. Gravity being one of the main issues to overcome when studying a granular medium, the experimental results presented here have been performed in a low-gravity environment. Experiments were boarded in the Airbus Zero-G from Novespace (www.novespace.fr), and the results presented obtained during parabolic flights. 2D cells containing the granular particles were mounted on a vibrated device and high-speed video recording was used to register and track the motion of each individual particles.

We will first report an experimental study on the free cooling of a granular medium made of beads: focusing on the time relaxation of the energy of the medium, and then, we will present similar experiments realized with disks in order to get access to the granular temperatures for the translation and rotational part of the particle's energy.

2. Free cooling

The cooling of a granular gas can be experimentally investigated by considering a granular medium submitted to a continuous external energy input (generally done by submitting the medium to a controlled vibration), then removing it and observing how the medium goes back to rest. Experimental studies on granular have to deal with gravity effects and studying model particles (disks in general) on an air flow table can overcome gravitational effects. Our approach was to perform experiments in a low-gravity environment by boarding the experimental apparatus in the Airbus Zero-G from Novespace. The airplane undergoes successive parabolic flights allowing around 22 s of microgravity per parabola. The relative gravity is recorded during the flight (**Figure 1**) allowing to monitor the quality of microgravity environment.

Irons beads with radius a = 1 mm enclosed in a 2D cell (**Figure 2**) have been used as model granular particles. The area fraction of the medium was $\phi_i = 19\%$. The cell was chosen with a circular geometry to ensure a homogeneous energy input into the system while submitted to the vibration. The walls of the cell are made of glass to cancel as much as possible electrostatic effects and to reduce undesired friction effects between the particles and the walls. The cell is mounted on a vibrating device ("Modal exciter, 100N, Bruel&Kjaer") to allow periodic (sine oscillations) external vibrations with different frequencies, ν, and amplitudes A. The maximum cell's velocities can be changed from 30 cm/s up to 250 cm/s. This experimental set up prevents us from density fluctuations found in fluidized beds or strong rolling contributions encountered when particles move over a horizontal vibrated plate. The motion of granular particles is recorded with a high-speed camera at 470 fps during 6 s in each experiment. About 3000 pictures (320 × 320 pixels) can be retrieved from each recording.

The high-speed video recording allows us to track each particle and then to get access to their positions inside the cell. From this knowledge, the dynamics of the medium can be retrieved through the velocities of each particle. The experimental processing is performed by image analysis [21]. Each particle p is tracked individually allowing to obtain the positions $x_p(t)$ and $y_p(t)$ as a function of time. It is interesting to note that from these sets of coordinates all experimental parameters required to describe the collective motion can be directly determined such as the velocities components, the normal restitution coefficient, e, but also the pair correlation function g(r) (**Figure 3**). The maximum of g(r) is found at the particle diameter

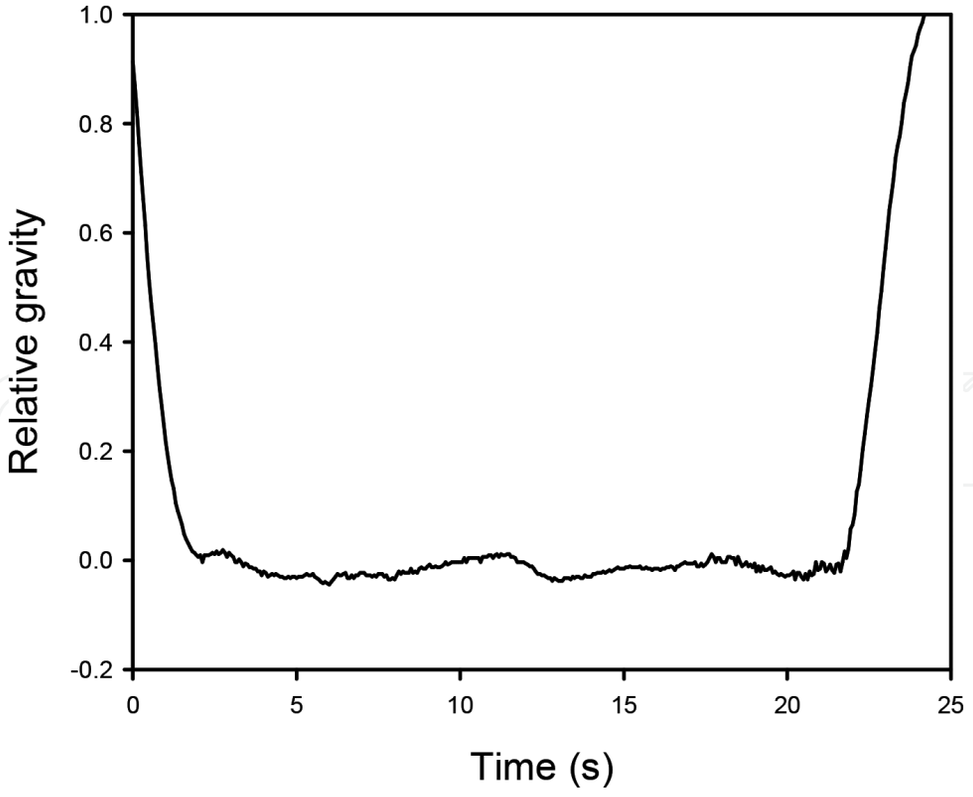

Figure 1. Typical behavior of the relative gravity during a parabola. These curves are used to check the quality of the microgravity environment.

http://dx.doi.org/10.5772/intechopen.68277

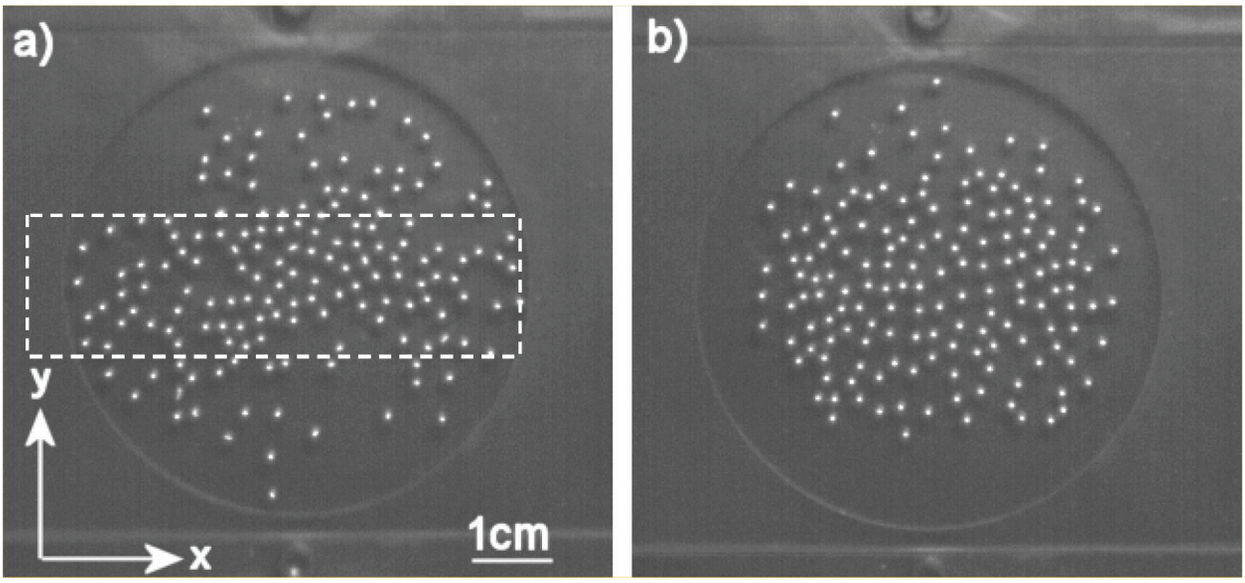

Figure 2. Snapshots of the experimental cell. The external vibration is applied along the y-direction (direction of the normal gravity). High-speed video recording is used to track the motion of each individual particle. (a) Vibration is on: the central part of cell contains an almost constant density of particles (dashed region). (b) The external vibration has been stopped and the overall motion of particles stops due to the inelastic collisions.

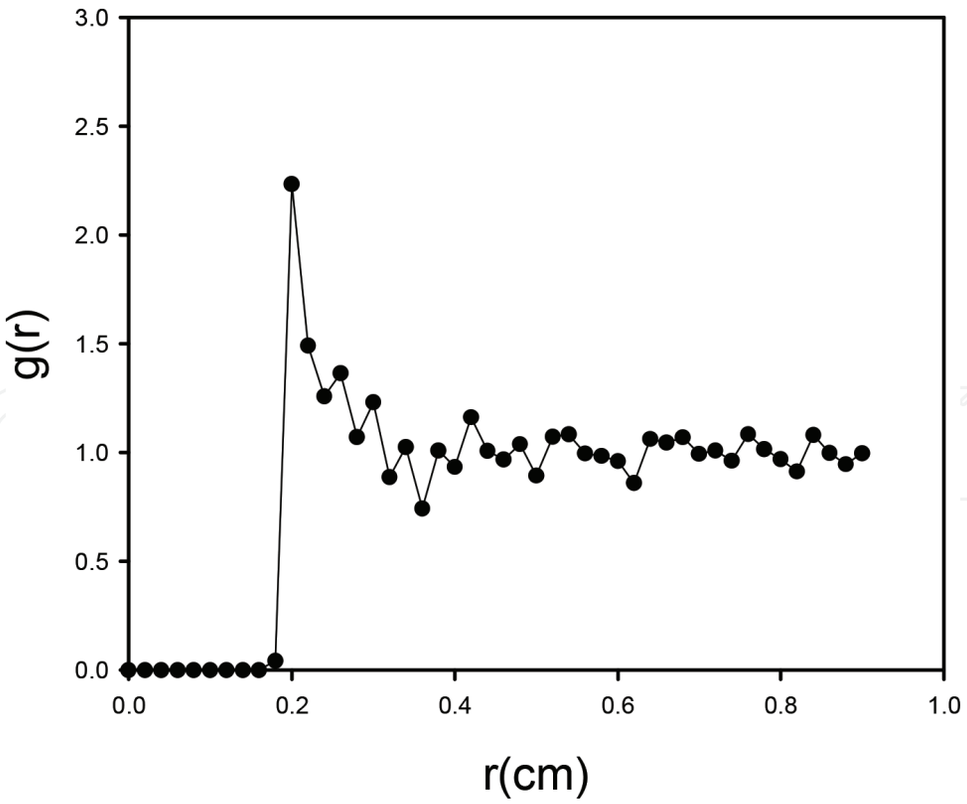

Figure 3. Experimental pair correlation function g(r) retrieved from the positions of the particles. This curve is averaged over all pictures recorded and on the spatial configurations of particles in the central area of the cell.

which proves that electrostatic effects are negligible. The small non-null value of the pair correlation function observed "before" the particle diameter is due to the uncertainty in the particle's position by image treatment.

In order to study the free cooling, that is, to relate the loss of energy of the medium due to the inelastic collisions between particles, the external vibration is switched on prior the micro-gravity occurs. In zero-g, the particles will then fill the entire region of the cell, and the video recording is started. After few seconds, the external vibration is switched off, and we observe the return to equilibrium (particles at rest throughout the cell). It is worth noting that in the presence of the vibration, two types of different regions clearly appear in the cell: two hot (and dilute) regions at the top and bottom of the cell while a dense region exists in the center of the cell (dashed area shown in **Figure 2a**). This experimental configuration gives us the possibility to study a homogeneous bed of particles in contact with two hot regions responsible for the energy input. As the external vibration is cancelled, the particles continue to move freely throughout the cell and tend to come to rest rapidly because of inelastic collisions between particles inducing energy loss. For cooled granular media, the formation of dense clusters of particles is often reported in experiments but it is not clearly observed in our situation: we rather observe some alignments of particles along "wavy lines" but there is no evidence of high and low-density regions as the main part of the energy loss is supposed to occur along the normal direction between two particles. The relative low area fraction of particles is also a possible reason for this non-observation of this clustering effect. Moreover, g-jitter still exists could add a general motion of particles in a given direction. But a short

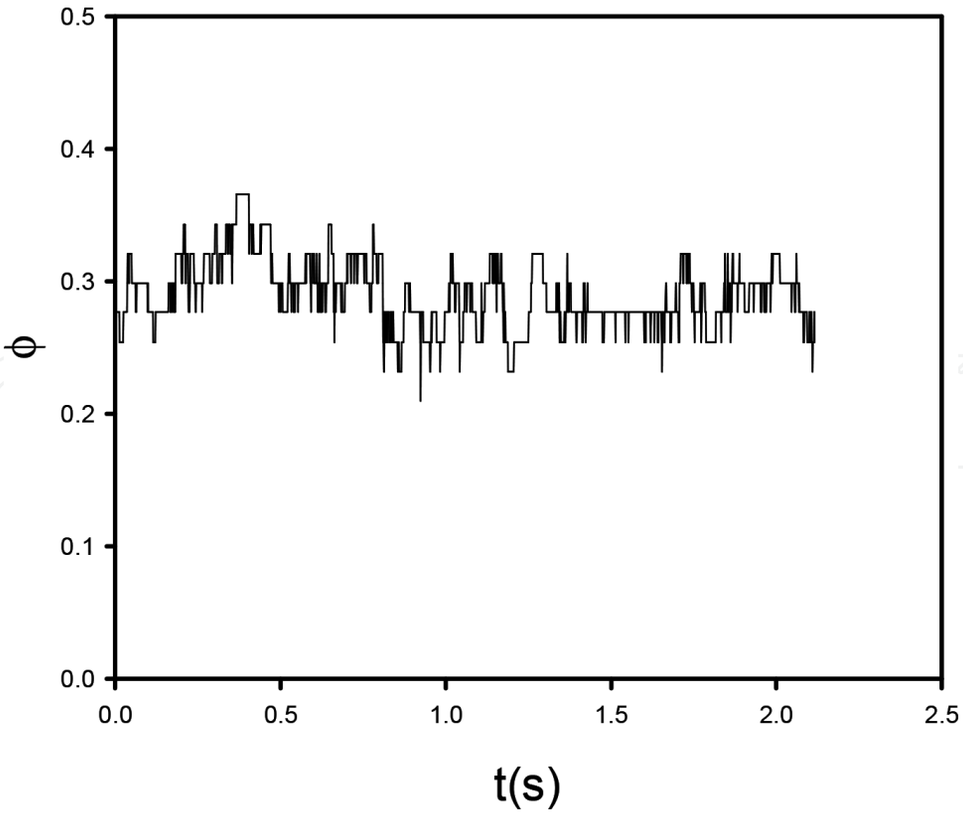

Figure 4. Volume fraction of particles in the central area of the cell as a function of the recording time (see **Figure 2a**). In this region, we will assume that the volume fraction of the granular medium remains constant.

time, after the vibration has been removed, we generally observe that the particles tend to stop in the center of the cell without evidence for clustering. During the recording, we have verified that the concentration in the central part of cell remains constant, and we have based all of other study on the dynamics of this area (**Figure 4**).

As the behavior of the medium is governed by inelastic collisions, we have determined experimentally the normal restitution coefficient as a function of the relative normal velocities of two colliding particles. A systematic investigation of binary collisions of particles has been realized either in the presence of the external vibration or without it. From the optical tracking and the knowledge of the trajectories, we can compute the directions and the magnitudes of the velocities before, $\overrightarrow{V_R}$ and after, $\overrightarrow{V'_R}$ an impact between particles. By tracking these changes in the direction of motion of each particle when a nearest neighbor is present, we are able to precisely determine the binary collisions from the trajectories and so the exact position of the colliding particles. It is then possible to consider the positions of particles around the location of the collision (**Figure 5**) and insure that the trajectories before and after collision are linear to

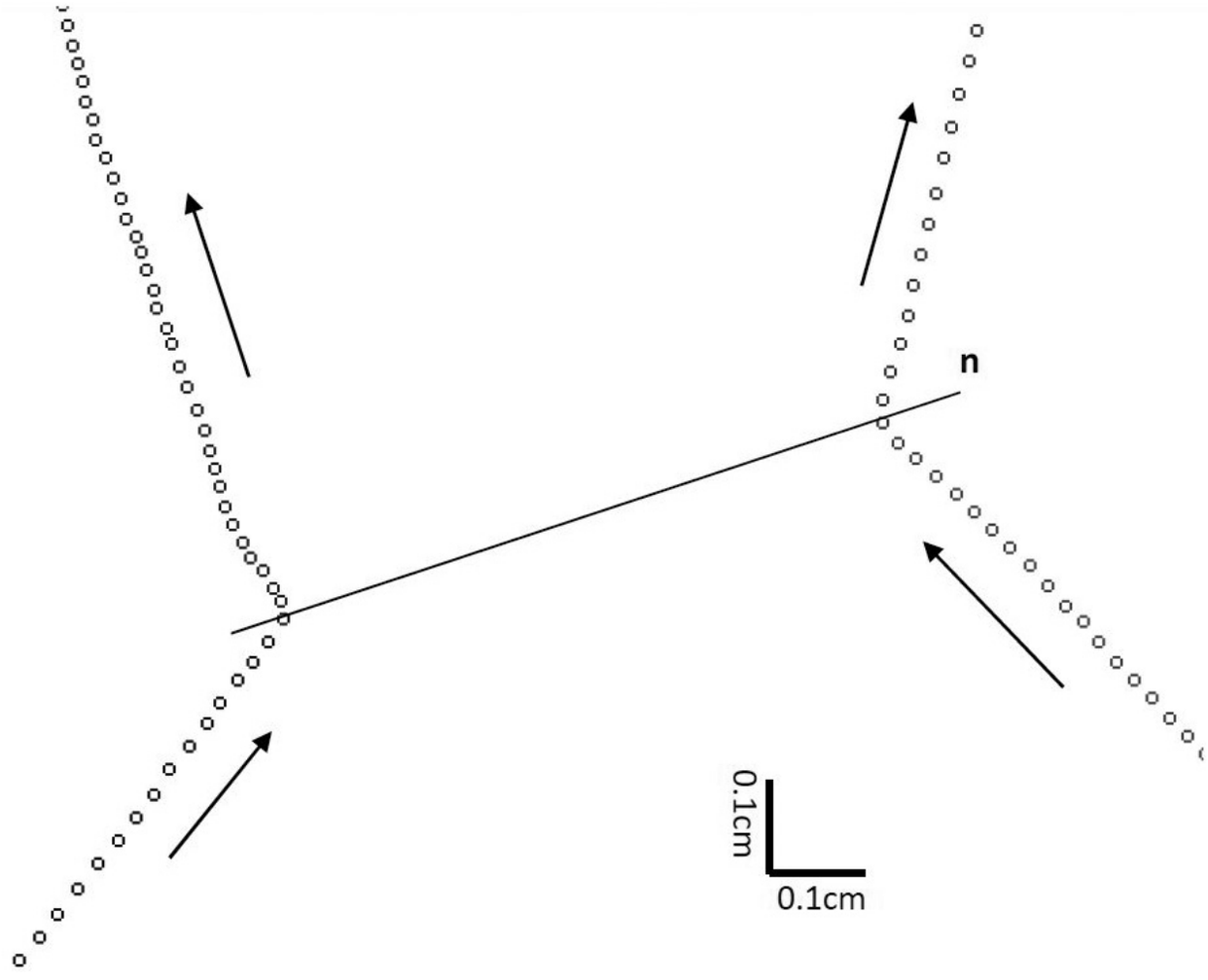

Figure 5. Experimental trajectories recorded during a binary collision between particles. The circles represent the positions retrieved from optical tracking. For a better understanding, we have added on the experimental trajectories the direction of motion (arrows) before and after collision. We can precisely obtain the position of each particle at impact and the direction of the normal direction n.

qualify this collision for processing. The direction of the normal direction at contact is then possible, and the restitution coefficient is obtained from $e = -|\vec{n} \cdot \overrightarrow{V'_R}|/|\vec{n} \cdot \overrightarrow{V_R}|$.

The behavior of the restitution coefficient vs. the normal relative impact velocity is presented in **Figure 6**. For high relative velocities, we obtain a value of the restitution coefficient of 0.9 (typical value for steel beads). The most amazing observation is that the restitution coefficient shows a sharp decrease for "small" impact velocity. This is a situation encountered in the case of wet particles when e = 0 for Stokes number $S_t = (mV_i/6\pi\eta a2)$ smaller than a critical value [22, 23]. This comes from the viscous dissipation but for dry particles, most experimental investigations report that the restitution coefficient increases for increasing impact velocities. Most of the experiments are made in labs (i.e., with gravity present) with impact velocities larger than 1 m/s (for a height h = 5 cm the impact velocity of a bead on the plane: $V_i = \sqrt{2gh}$ is already 1 m/s). The restitution coefficient between two dry beads attached by strands in a pendulum device has also been studied [24], where it has also been found that a low value of the restitution coefficient was reported at low velocities (typically below 20 cm/s), and such behavior is well confirmed in our study without experimental drawbacks.

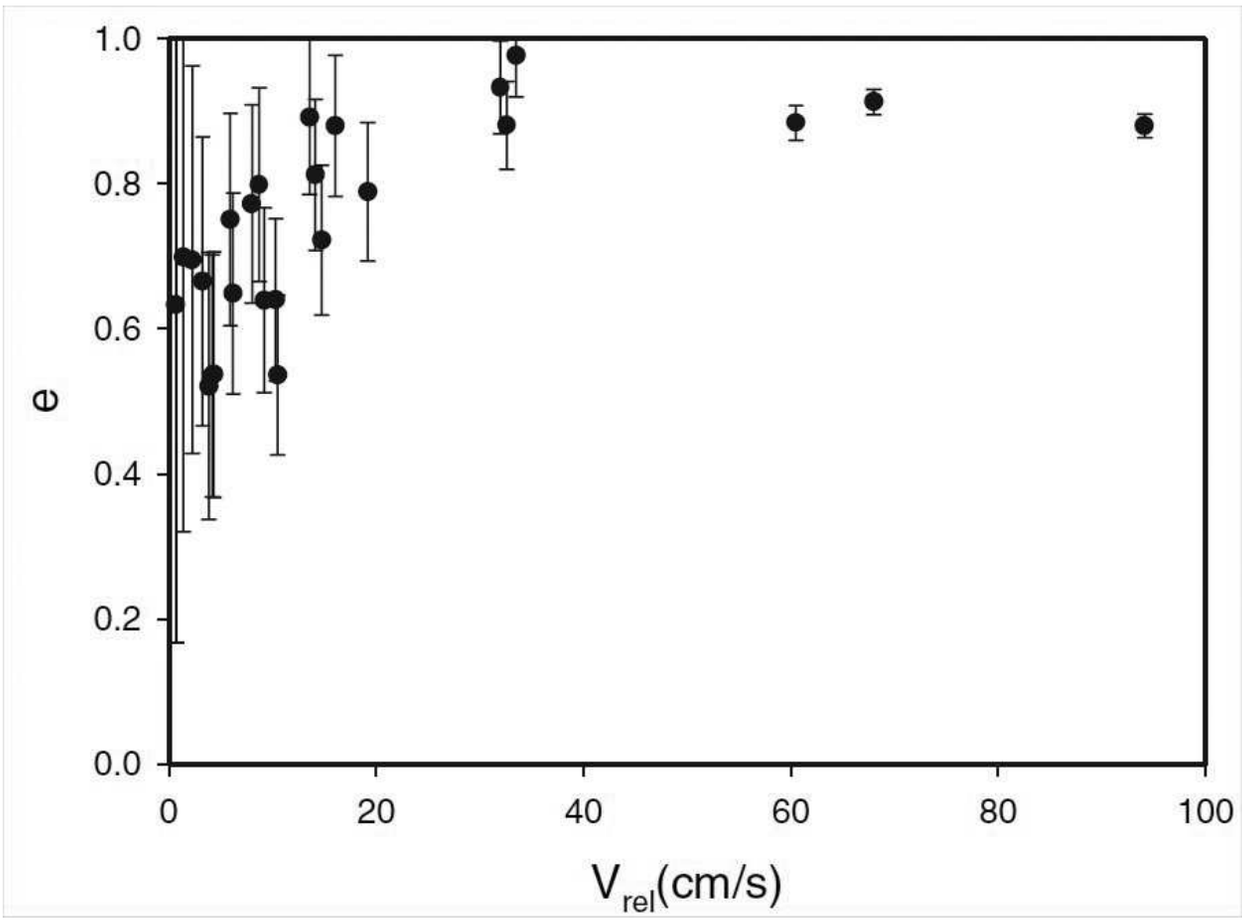

Figure 6. Experimental dependence of the normal restitution coefficient, e, as a function of the relative normal impact velocity, obtained from the experimental trajectories of the particles. A clear decrease at low impact velocities is observed.

To investigate the free cooling more precisely, a typical record on how the energy decreases once the external energy input has been cancelled is presented in **Figure 7**. This behavior is monitored through the average velocities of the particles in the central area of the cell. One can observe the rapid decay of the average velocity. The non-zero value measured for "long times" comes from the small gravity fluctuations occurring during the parabolic flight.

We can first consider the energy decay assuming a constant restitution coefficient (typically e = 0.9 for stainless steel beads). The time dependence of the energy is predicted to behave as $E(\tau) = 1/(1+\tau)^2$, $\tau = (1-e^2)t/t_E$, where t_E is the Enskog time [25]: $t_E = (a\sqrt{\pi})/\left(\sqrt{2}\phi V_0 g(r)\right)$. V_0 is the initial average velocity in the medium. With our experimental set up, we can determine experimentally all the parameters involved. A quantitative comparison with experiments is presented in **Figure 8** (squared symbols) for a cell velocity of 75 cm/s and with the following experimental values: $\phi = 0.297 \pm 0.027$, $V_0 = (0.11 \pm 0.01)\ m/s$ and $g(r = 2a) = 2.23 \pm 0.02$. The drop of energy found from experiments is much faster than the theoretical one while considering a constant restitution coefficient. A possible explanation may result from the friction of the particles on walls of the cell, introducing an additional loss of energy. Nevertheless, a precise and systematic analysis of the trajectory of a single particle after the vibration has been cut off shows a linear motion at constant speed between two collisions of particles; we may then reject this possibility. The Enskog collision time is $t_E = 0.0172\ s$. In order to check this value, we

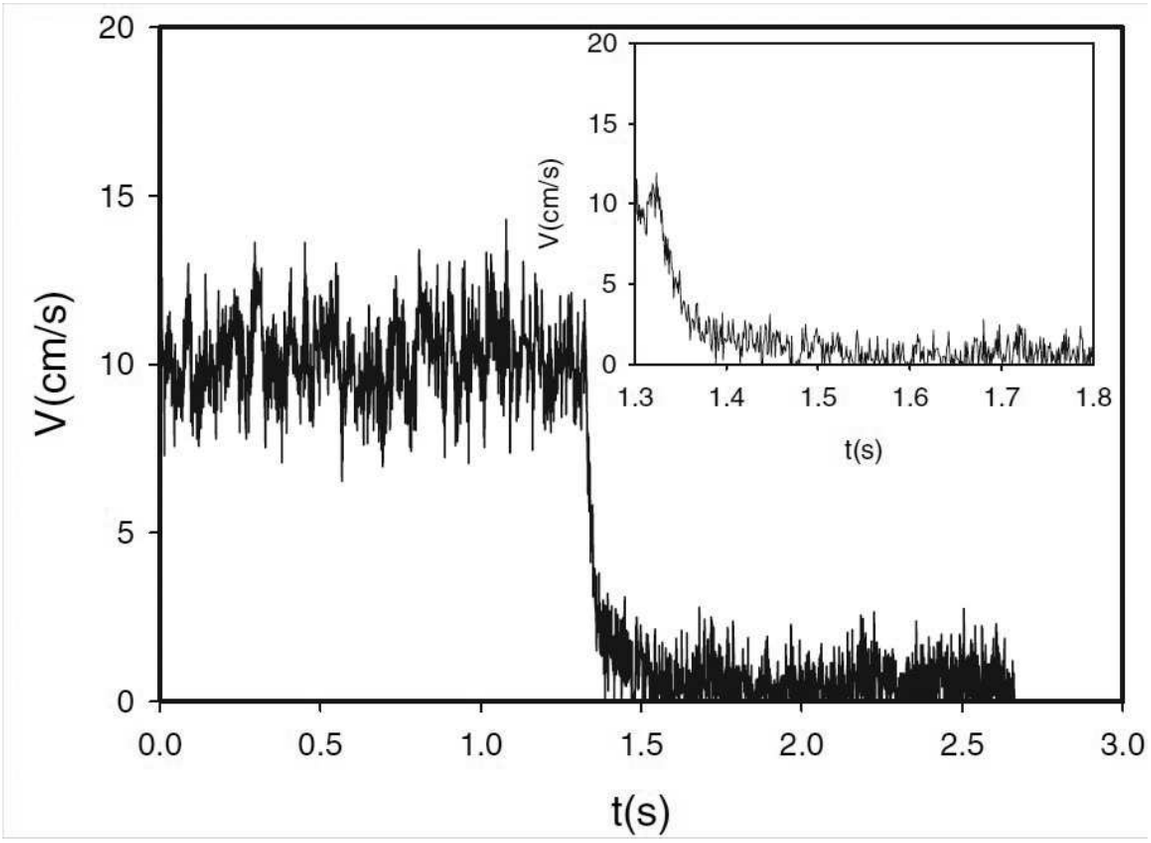

Figure 7. Average translational velocity as a function of time obtained in the central region of the cell. The vibration is removed during the microgravity period. A clear decrease of the energy can be observed (max cell velocity of 74.6 cm/s).

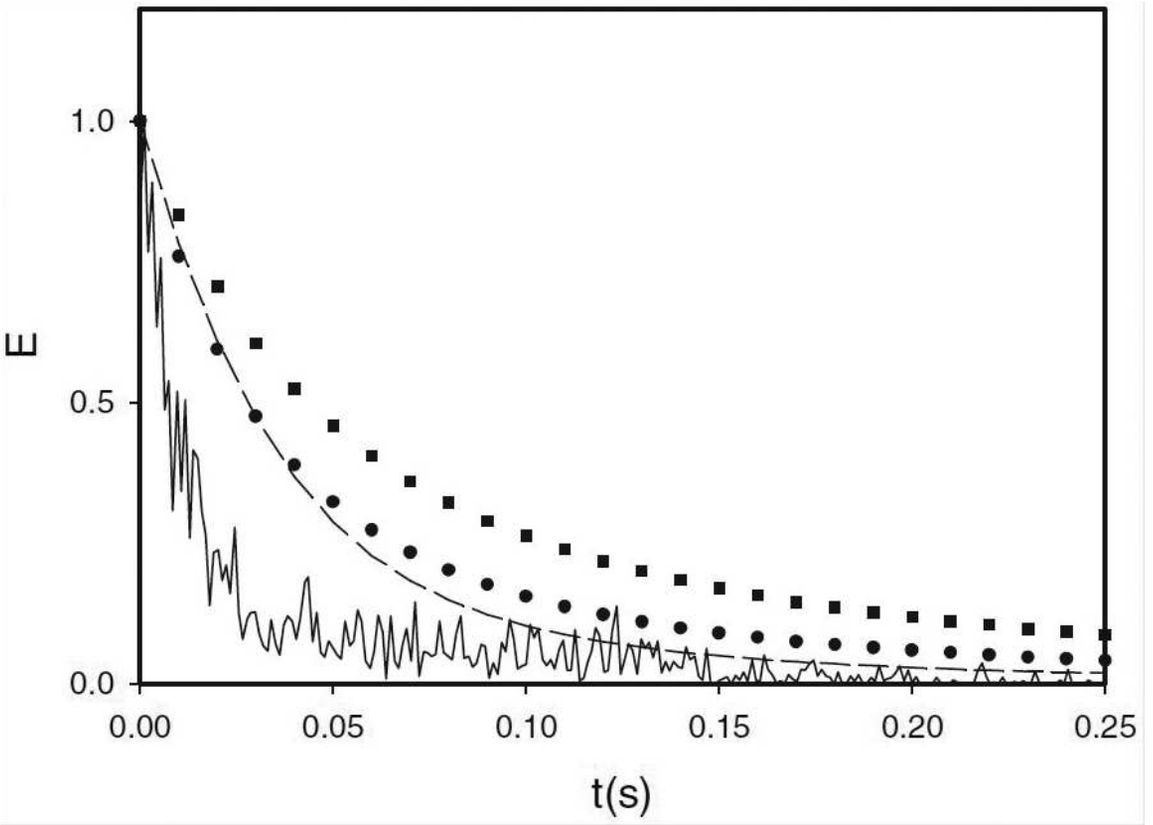

Figure 8. Experiments (plain curve) and theory of the energy decrease. Squares: theory including a constant restitution coefficient. Circles: theory considering the rotational energy. Dashed line: theory focusing only the translational energy but including the velocity dependence of the restitution coefficient (see **Figure 6**).

have performed a large statistics on our experiments to obtain the average time interval separating two consecutive collisions in the central part of the cell. We found an average time interval of (0.0127 ± 0.0021) s by direct measurements in rather good agreement with the theoretical value.

So, the possible discrepancy between energy decays observed experimentally and the predicted one by theory may come from the rotational kinetic energy which also dissipates a part of the energy through the surface roughness of the particles [26]. To get a complete description of the binary collision, we have introduced a tangential restitution coefficient, β, in order to characterize the contribution of the rotation of the particles. The time dependence of the translational and rotational energy is obtained from coupled differential equations (Eq. (15) in Ref. [26]): note that the parameters considered in this description are all retrieved from experiments, except β. This system of equations was solved numerically. We have introduced our experimental results for the inelastic parameters of particles and setting $\beta = 0.1$ (**Figure 8**, black circle—if we cancel the rotation, that is, $\beta = -1$, we recover the situation of a constant normal restitution coefficient). We see that the energy decreases more rapidly but it seems that the rotational kinetic energy has limited impact whatever the value of the tangential restitution coefficient and it is still not enough to represent the experimental behavior.

To improve the agreement between theory and experiments, we may consider the velocity dependence of the restitution coefficient. We can express the rate of decrease of the

translational kinetic energy T like $dT/dt = -n_c(1 - e2)T$ with n_c the rate of binary collisions. In 2D, $n_c = \left(2V\phi g(r)\right)/(\pi a)$ with V, the average velocity. Moreover, introducing the normalized energy $E = T/T_0$ and the velocity ratio $V/V_0 = T/T_0$, the rate of decrease of energy can be rewritten in the form:

$$\frac{dE}{dt} = -\frac{g(r)\phi V_0}{a}\sqrt{\frac{2}{\pi}}\left(1 - e(E)^2\right)E^{3/2} \tag{1}$$

But now e is assumed to depend on the normal relative velocity. We may assume that the average relative velocity is of the same order as the average velocity; then from **Figure 6**, we can obtain the following trend $e(E) = 0.82 - 0.5e^{-2.5E}$. Substituting this last relation in Eq. (1) and solving it numerically gives the behavior presented in **Figure 8** (dashed line). Compared to the case including the rotation, we observe a more pronounced decrease of the energy with time. This is understandable since we observed that during cooling the restitution coefficient decreases, increasing the loss of energy. Equation (1) is obtained from a rough approximation based on the average velocity, while the probability distribution may be considered. Moreover, the tangential coefficient may probably also be dependent on the relative angular velocities of colliding particles.

This first approach on the dynamics of a granular medium shows interesting results but as stated before, the analysis is not complete due to the lack of consideration on rotational effects. With beads and our experimental setup, accessing these data is not possible. We will then introduce in the next part recent experimental investigations based on the same principle but replacing beads by disks in order to obtain a complete description of the dynamical behavior.

3. Translational and rotational temperatures

In this part, our aim is to provide experimental data both for the normal and tangential restitution coefficients and for the different quantities related to the rotational and translational degrees of freedom such as the distribution functions and the rotational and translational temperatures. As introduced previously, the kinematics of granular particles submitted to a vertical vibration will still be used in a low-gravity environment. We shall particularly focus on the ratio between rotational and translational temperatures. Several other groups have already presented experimental results on granular flow under such conditions [27–30], but to our knowledge, this is the first experimental study giving access to rotational and translational velocities and so the corresponding temperatures.

We have used the same 2D cell from the previous part by now with a rectangular shape made in Duralumin. The cell has a height $L_y = 6.8$ cm and a width $L_x = 6$ cm. The particles studied were brass disks having a diameter $\sigma = 6$ mm (radius a = 3 mm) and mass $m = 4.6{\cdot}10^{-4}$ kg. The initial area fraction ϕ of the medium is obtained from the number of disks N (12 or 24, i.e., area fractions of 8.3 or 16.6%). For this experimental study, we chose this rectangular shape in order to easily monitor the energy input into the medium. The external vibration is still periodic (sine oscillations) with different frequencies, ν, and amplitudes A, and it is still

applied along the y-direction (which is the direction of normal gravity). In order to increase the precisions of experimental data, the video recording is performed during the whole parabola with a higher frame rate (i.e., 900 fps) and higher image resolution (720 × 720 Pixels); each record gives access to around 22,000 pictures per parabola. To reduce the effect of friction between the disks and the glass plates of the cell, we have added three small steel beads on each side of a disk. In addition, it also reduces the tilting of the disks when the external vibration is on. The key question being now the rotational aspects, each disk is pierced with two small holes, symmetric about the center of the disk and video observations are realized by light transmission (**Figure 9**).

This set up grants us with images having a high contrast and quality. The position of the disk is retrieved from the tracking of the two holes for each disk as a function of time. The barycenter of the holes gives access to the x- and y-position of the disk and by following the variations of these positions as a function of time to the components of the velocity $v_x(t)$ and $v_y(t)$. Nevertheless, by computing the time dependence of the angle $\theta(t)$ (**Figure 10**) (obtained from the angular position of the holes about the horizontal), allows to retrieved the angular velocity $\dot{\theta}(t)$.

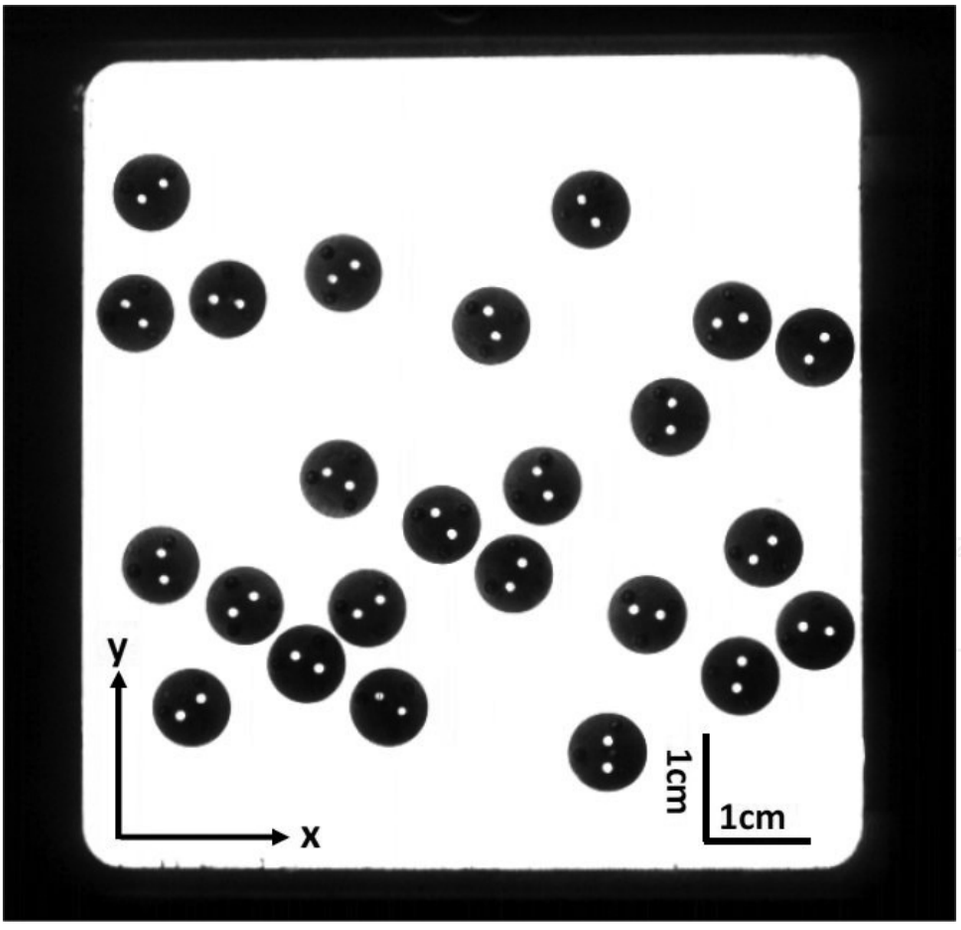

Figure 9. Picture of the medium recorded in microgravity when being submitted to the external vibration (along the y-direction). Optical observations are performed from light transmission. The two holes can be clearly identified. A side and top sketch of one disk is also shown.

http://dx.doi.org/10.5772/intechopen.68277

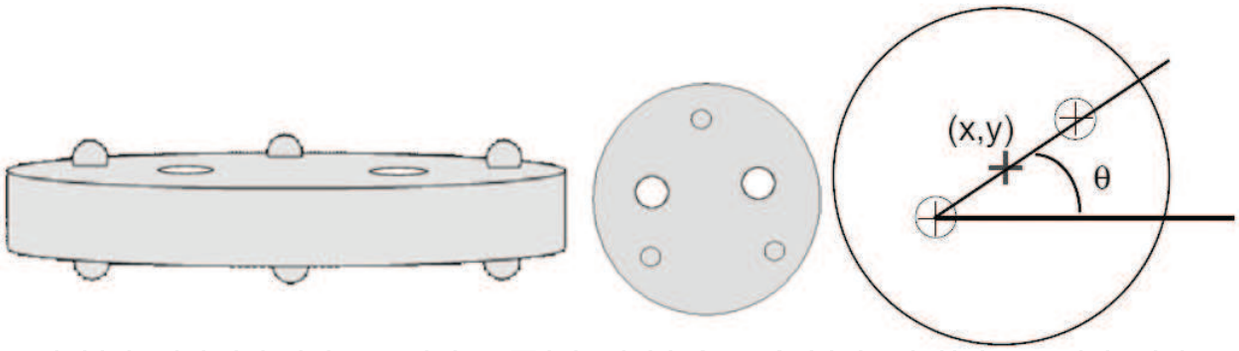

Figure 10. Disks used as the granular particles. Light transmission allows very high contrast pictures. The optical tracking of the two holes of a single disk permits to compute the orientation angle of the disk as a function of time.

The orientation angles of the disks can be fully determined from 0 to 360 degrees. A typical experimental record of θ(t) is presented in **Figure 11**. On such record, a sharp change in the direction of rotation (positive or negative slope) or a significant change in the slope is the proof that a collision occurs with another particle. On the contrary, when the particle experiences no collision (e.g., time larger than 5 s in **Figure 11**), the angular velocity remains quite constant, indicating the absence of friction with the lateral walls. During a parabolic flight, the aircraft is subjected to g-jitter along the three directions (**Figure 1**). Experiments were submitted to g-jitter with period of fluctuations of about 1 s and amplitudes of about 0.01 g (**Figure 1**). Although these fluctuations may play a role during the collision of the particles with the moving walls of the cell, they have limited impact on the motion of particles located in the central region of the cell where experimental data were retrieved. Moreover, a systematic

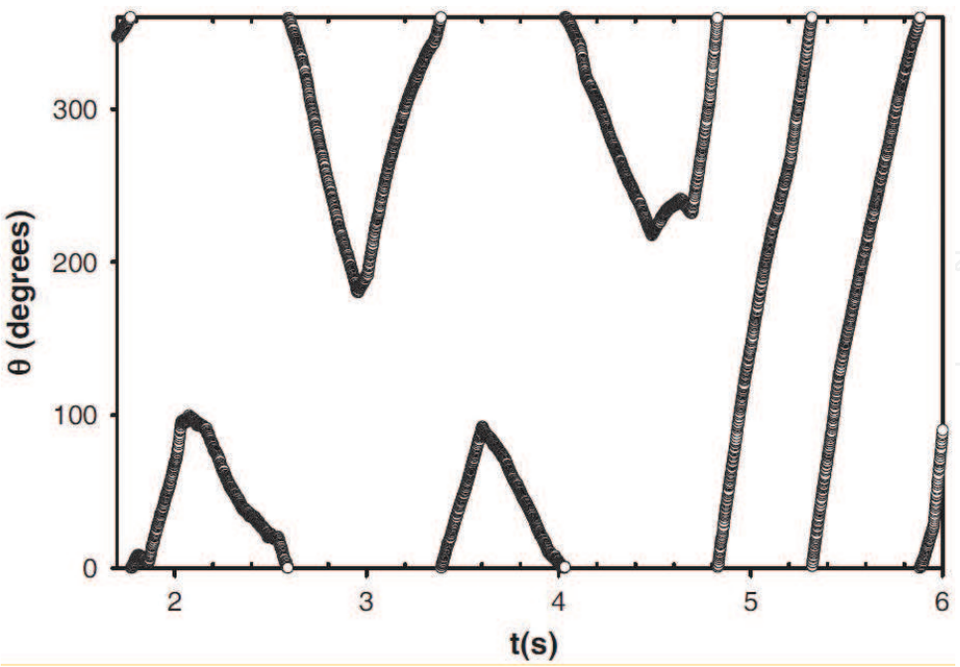

Figure 11. Experimental record of the angle of orientation, θ(t) of a disk when both microgravity and external vibration are present. Collisions can be clearly identified from a change of rotation or value of the angular velocity (i.e., The slope).

analysis of inelastic parameters (normal e, and tangential β, restitution coefficients) was achieved by analyzing the trajectory of each disk.

The collision between disks is processed as we did for the beads in the previous part except that now, the relative velocity includes the rotational part $\overrightarrow{V_R} = \overrightarrow{v_1} - \overrightarrow{v_2} - a(\dot{\vec{\theta}}_1 + \dot{\vec{\theta}}_2) \times \vec{n}$ where the subscripts 1 and 2 stand for the two colliding particles at a given time. Again, the normal restitution coefficient is obtained through $e = -|\vec{n} \cdot \overrightarrow{V'_R}|/|\vec{n} \cdot \overrightarrow{V_R}|$ and the tangential restitution coefficient by $\beta = -|\vec{n} \times \overrightarrow{V'_R}|/|\vec{n} \times \overrightarrow{V_R}|$. Another way to express the tangential restitution coefficient is to introduce the angle γ between $\vec{n}$ and $\overrightarrow{V_R}$ (**Figure 12**), we have for disks the relation [31]: $1 + \beta = -3(1 + e)\mu \cot(\gamma)$. The initial slope of β versus cot (γ) allows the computation of μ, the friction coefficient.

We have obtained experimentally an average value of $e = 0.64 \pm 0.03$. Although it is sometimes noticed in such situation [24, 32], we did not observe for the disks we used any clear dependence of e on the relative impact velocity. The experimental determination of the restitution coefficient α, between a particle and the walls of the cell reports a value $\alpha = 0.71 \pm 0.04$. We were also able to determine the behavior of the experimental tangential restitution coefficient as a function of $cot(\gamma)$.The results are presented in **Figure 13**. From the initial slope, one can compute an average value for the friction coefficient when particles are at contact: $\mu = 0.14 \pm 0.01$. As most of the binary collisions are head-on collisions (due to shape of the experimental cell), we have decided to take an average value of the tangential restitution $\beta = 0.7 \pm 0.05$.

The density and local velocity profiles of particles within the cell can be determined again from the positions of particles. In **Figure 14**, we have plotted the profiles of the x- and y- components of the disks' velocity. The area fraction of particles in the center of the cell is almost twice the initial one while close to the top and bottom walls, the value found is smaller. This is directly related to the inelastic nature of collisions which form clusters of particles [33, 34]. For this

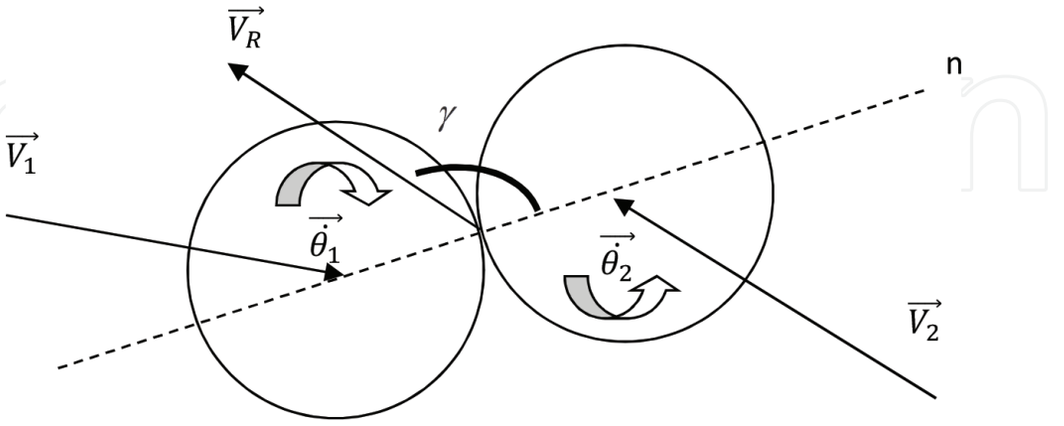

Figure 12. Sketch of a binary collision. $\overrightarrow{v_1}$ and $\overrightarrow{v_2}$, and $\dot{\vec{\theta}}_1$ and $\dot{\vec{\theta}}_2$ represent, respectively, the linear and rotational velocities of the particles before and after impact. $\overrightarrow{V_R}$ is the relative velocity and n the normal direction at collision. The impact angle γ is defined from n to $\overrightarrow{V_R}$.

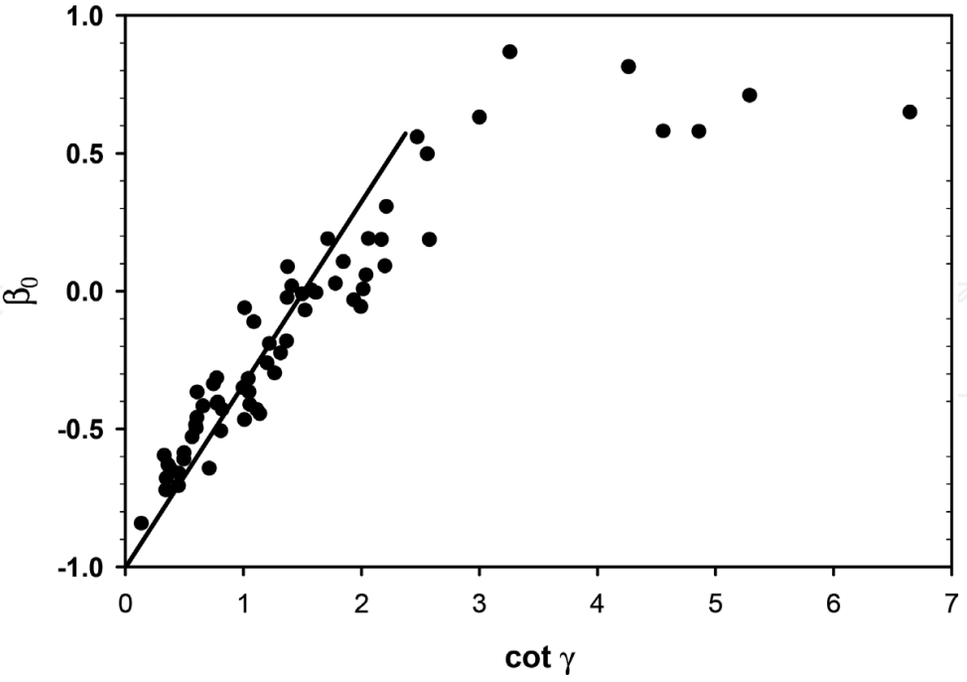

Figure 13. Experimental behavior of the tangential restitution β as a function of $cot(\gamma)$, where γ is the angle between the normal direction at contact and the direction of the relative velocity. The plain line is a linear regression used to compute the value of the friction coefficient when particles are at contact.

experimental study, the cell may again be divided into two different and well-identified regions [35]: a central one that we will refer as the "cold" area and the ones close to the top and bottom walls (where the energy is injected into the medium), referred to "hot" areas. In the following, subscripts H and C will be used, respectively, to identify the "hot" and "cold" regions of the cell. Considering all experiments, we have noticed first that the values found to characterize the "hot" zone by the height h_H were not related to the amplitude of vibration as one could expect, and second that an average value $h_H = 9$ mm ≈ 3.5a was acceptable in our experimental situations. Moreover, computation of the mean free path of particles in the "cold" zone gives a distance of about 12a (when using 12 disks) and 6a (for situations with 24 disks). These statements are found by considering the density of the "cold" region where typical values are found to be 13% (12 disks) and 30% (24 disks). We may conclude that the behavior of particles in the "cold" area is mainly governed by particle-particle collisions. We do not meet situations in which particles are moving through the bulk without being struck by another particle. Last, checking experimentally how the density profiles evolve with time does not present low-frequency oscillations like the situation reported in Ref. [36].

The temperatures of the granular medium are retrieved from the velocities of particles and from both contributions: the translation $T_{tr} = mV^2/2$, and the rotation $T_{rot} = I\omega^2/2$ (I the moment of inertia). In steady state, the temperature is calculated from a balance between two opposite fluxes: the energy brought to the medium by the particles in the "hot" areas of the cell and the dissipation in the bulk (i.e., the "cold" region). All experimental data presented below were retrieved from the "cold" region. To obtain reliable values, the whole set of the 20,000 images recorded are treated for each experimental value reported in this paper. We may also

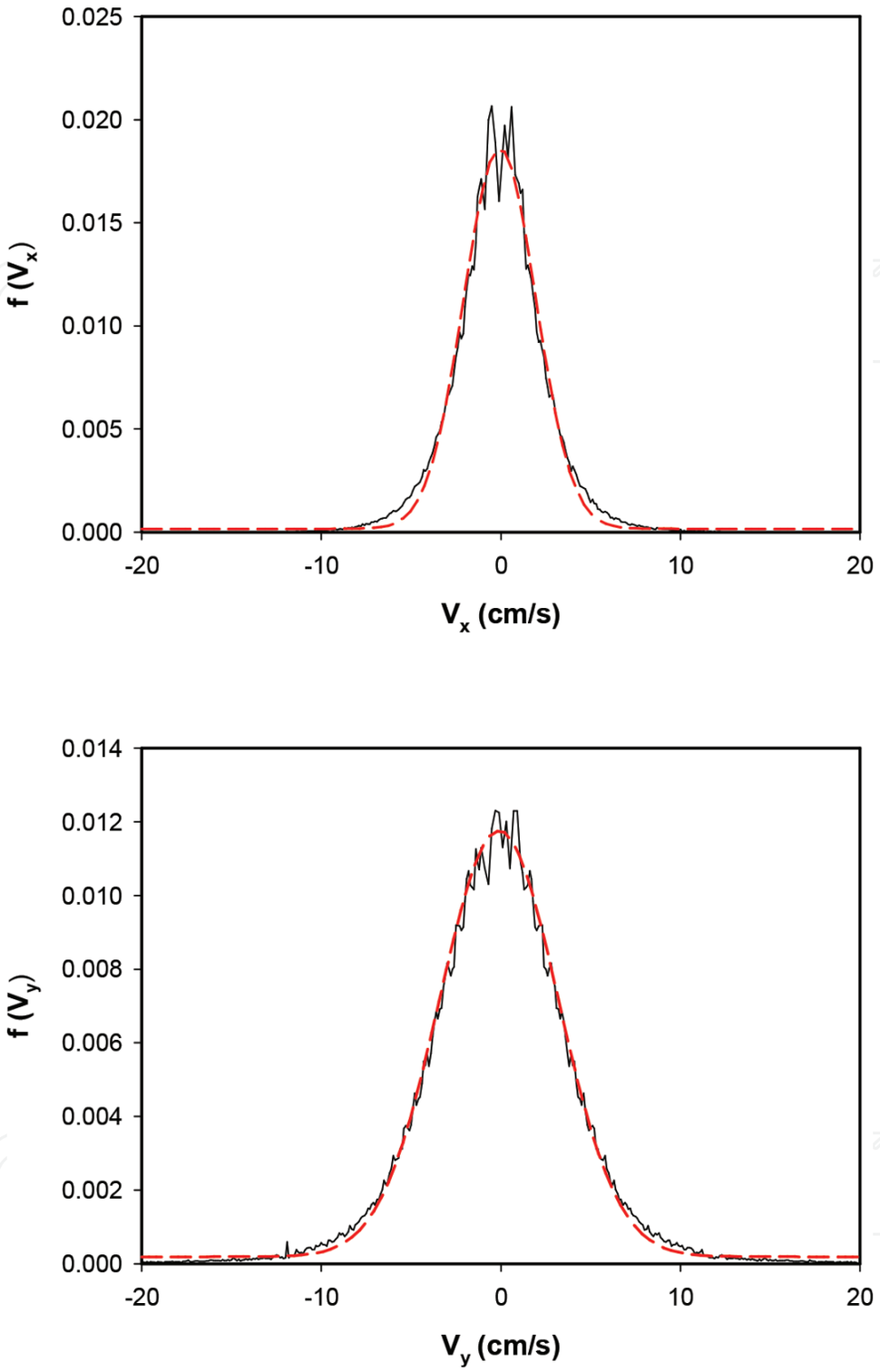

Figure 14. Velocity distributions of the component along the direction of vibration (y-direction) and transverse to it (x-direction). The experimental curves are drawn with plain lines. The dashed lines correspond to a Gaussian plot with the average velocity determined experimentally.

consider an undesired effect of g-jitter arising in parabolic flights but we will take it into account when comparing experimental results with theories. An average number N_H of particles present in the "hot" regions can be obtained directly from the density profiles at any time.

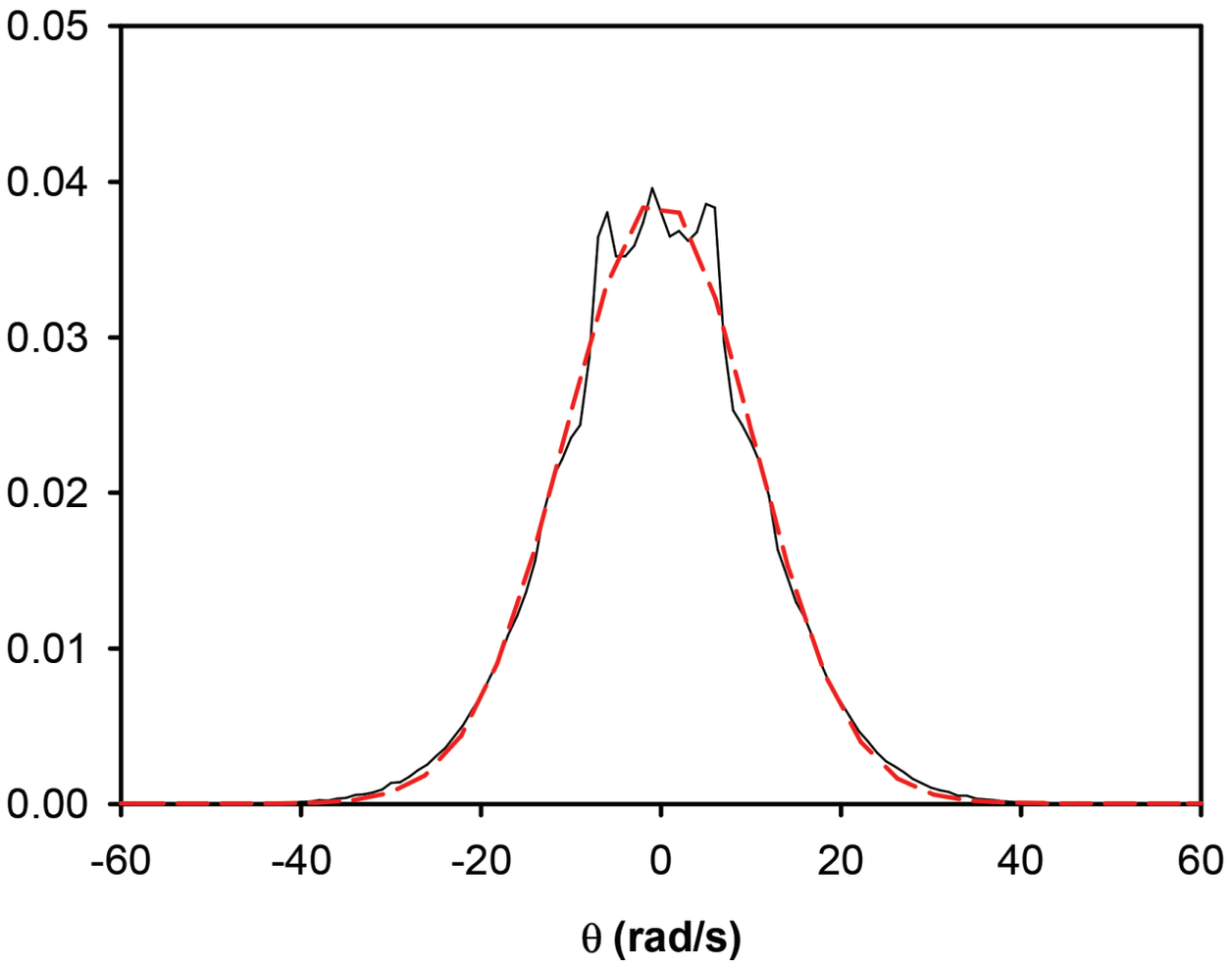

Figure 15. Typical angular velocity distribution of the particles (experiment: plain curve). The dashed line corresponds to the mathematical plotting of a Maxwell distribution, which includes the average angular velocity determined experimentally.

Typical experimental distributions for translation and rotational velocities are shown, respectively, in **Figures 14** and **15**: A Gaussian behavior can be observed. The dashed line on the figures represents the plots of the Gaussian distribution in which the experimental values of the squared velocities have been introduced, and one can notice the good agreement.

Due to the rectangular shape of the experimental cell used and to the relatively low area fraction, the main contribution to the temperature was expected to be found along the direction of the external vibration (the $y-$ direction). The temperature ratios T_y/T_x and T_{tr}/T_{rot} with $T_{tr} = (T_x + T_y)/2$, in terms of the maximum cell's velocity $A\omega$ ($\omega = 2\pi$n) for the two area fractions used, have been calculated. One may note that the ratio T_{tr}/T_{rot} is not drastically affected if one considers only T_y as the only contribution to the energy. For the fraction area of 16.6%, the ratio T_{tr}/T_{rot} is ranging from about 4 to 10, respectively, for maximum cell velocity from 20 to 40 cm/s, while T_y/T_x goes from 2 to 4 at maximum, while for the lowest fraction area (8.3%), T_{tr}/T_{rot} is ranging from 11 up to 24 and T_y/T_x from 5 to 7 only under the same conditions of maximum velocities. We shall analyze these experimental results by focusing first on the ratio T_y/T_x which is clearly dependent on the area fraction of the medium (the larger the ratio, the smaller the area fraction). Without any surprise, the temperatures obtained

along the direction of the vibration are always larger than the ones in the transverse direction. This comes from the fact that the main part of energy injected is along the y-direction, and the relatively low area fraction does not allow the redistribution of this energy toward the perpendicular direction. At low area fraction, the particles can move easily and the y-direction drives the general motion. On the other hand, we also observe a net increase of the ratio T_y/T_x with the driving velocity of the cell, but less pronounced for the lower area fraction. However, the driving velocity is not the only parameter of the problem and the amplitude can also play a role. For example, the ratio $T_y/T_x = 1.98$ found was obtained for the smallest amplitude ($A = 0.556$ mm) and the largest frequency (60 Hz). Under the conditions of high frequency but small amplitude, we clearly see a concentration of particles in the central area of the cell, and consequently, the corresponding energy input is small. It then explains the low ratio found in such experiment, to be compared to a similar value of $A\omega = 0.22$ m/s but with much larger amplitude ($A = 2.3$ mm). We have set the frequency scale between 10 Hz and 30 Hz, and the corresponding amplitudes of vibration used are large enough to avoid the aggregation of particles in the center of the cell. Last, we can clearly identify the "cold" area straight from the density profiles. The second result is related to the ratio T_{tr}/T_{rot} which obviously increases with $A\omega$ and which is also dependent on the area fraction. The translational temperature is quite one order of magnitude larger than the rotational temperature. Because almost all collisions between particles are quite, head-on as reflected by the high value of T_y/T_x, can explain why the transfer from translational to rotational energy is rather weak, mainly at the lowest area fraction.

As a first step to describe the experimental behavior on granular temperatures, we can use existing theoretical models using a mean-field theory [37]. In this description, the rate of change of the temperature of a granular medium is determined through two coupled equations

$$\begin{cases} \dfrac{dT_{tr}}{dt} = J_{dr} + G[-AT_{tr}^{3/2} + BT_{tr}^{1/2}T_{rot}] \\ \dfrac{dT_{rot}}{dt} = 2G[B'T_{tr}^{3/2} - CT_{tr}^{1/2}T_{rot}] \end{cases} \tag{2}$$

where T_{tr} and T_{rot} represent, respectively, the translational and rotational temperatures, and $G = \frac{16}{\sigma\sqrt{\pi m}}\varphi g_2(\varphi)$ is related to the collision rate between particles; $g_2(\varphi)$ being the pair correlation function at contact. In two dimensions, $g_2(\varphi) = (1 - 7\varphi/16)/(1 - \varphi)2$. A, B, B', and C are constants, which depend only on the inelastic properties of the particles [38]. J_{dr} is the energy flux input into the medium and a homogeneous input of energy into the medium is assumed. These four constants are positive so that the minus signs are related to the loss of energy during the collision of particles. We state that the driving energy is acting on the translational temperature because of the preferred collisions with normal incidence. We may note that when the rotation mainly governs the behavior of the granular, J_{dr} is included in the second equation of (2) [39, 40].

Several inelastic modelizations were proposed by Herbst et al. [38] going from a simple consideration of a constant tangential restitution coefficient up to more complex ones where the tangential restitution depending on γ_{12} (the contact angle obtained neglecting the rotational velocities) or on the real contact angle γ. From the second equation of Eq. (2), the energy ratio T_{tr}/T_{rot} can be obtained considering the medium in steady state $dT_{rot}/dt = 0$, allowing to get the

relation $T_{tr}/T_{rot} = C/B'$. In this equilibrium regime, $dT_{tr}/dt = 0$ and replacing T_{rot} in the first equation of Eq. (1) also give $T_{tr} = [CJ_{dr}/G(AC - BB')]^{2/3}$. Depending on the model used, the expressions of the constant C and B' can be evaluated and only depend on the inelastic properties of particles and to their inertia; however, the area fraction or the driving energy flux J_{dr} is never considered. Using our experimental values for the normal and tangential restitution and friction coefficient, we can numerically solve the models. Results show values of the ratio of T_{tr}/T_{rot} at maximum of 5, and more importantly, the results are not dependent on the maximum velocity of the cell. These models do not deal with an anisotropic temperature because their predictions are usually compared to numerical simulations where the energy is supposed to be added into the medium isotropically. This is why these models cannot represent our results.

When an external vibration is acting on the granular, it can be viewed as a medium which dissipates energy while energy is added into it through the vibration per unit time. The equilibrium temperature (and state) can be found from the equilibrium equation $J_{dr} + Q_d = 0$, where J_{dr} is the energy flux injected in the medium by the collisions of particles with the walls of the cell and Q_d, the energy flux dissipated during the binary collisions between particles. J_{dr} is found to act in the "hot" areas of the cell, while Q_d is computed in the bulk. The results obtained from experiment and geometry clearly show that the main energy input on particles occurs along the direction of the vibration. From our observations, we have considered the areas of energy input by defining two layers of thickness h_H and having the same width L_x. Then, the particles' density is much smaller than the one of the medium, and we have introduced N_H as the average number of particles present at any time. Thus, the bulk of the medium (i.e., the "cold" zone) reduces to dimensions $h_C = L_y - 2h_H$ where only $N_C = N - 2N_H$ particles are present at any time; the surface of this zone is then $S_C = h_C L_x$. In the "cold" zone, the dissipated energy depends on the collision frequency $f_E(T)$ which in turns depends on the temperature T of the medium $T = m\langle v_x^2 + v_y^2\rangle/2$. If we neglect the loss of energy coming from tangential restitution coefficient, the energy dissipated per collision is given by:

$$\Delta E_{pp} = m\frac{(e2-1)}{4}\langle[(\overrightarrow{v_1} - \overrightarrow{v_2})\cdot\overrightarrow{n}]^2\rangle = \frac{(e^2-1)}{2}T \tag{3}$$

The frequency collision which is the inverse of the Enskog time is given in 2D by $f_E = \sqrt{2\pi}\frac{N_C}{S_C}\sigma g_2(\varphi)\langle v\rangle = \frac{2}{N_C}f_E^N$ where N_C/S_C represents the number density in the "cold" region and f_E^N is the number of collisions between N particles per unit time. Finally, the dissipated energy flux will be expressed as follows:

$$\begin{aligned} Q_d &= f_E^N \Delta E_{pp} = \frac{N_C^2}{h_C L_x}\frac{1-e^2}{2}\sigma g_2(\varphi)\sqrt{\frac{\pi}{m}}T^{3/2} \\ &= \frac{N_C^2}{h_C L_x}\frac{1-e^2}{4}\sigma g_2(\varphi)\sqrt{\frac{\pi}{m}}T_y^{3/2}\left(1+\frac{T_x}{T_y}\right)^{3/2} \end{aligned} \tag{4}$$

To express the energy input into the medium, we must now take into account the flux coming from the collisions between the particles and the walls of the cell. When a collision occurs, the

kinetic energy change for one particle is: $\Delta E_{pw} = m(v\prime_y^2 - v_y^2)/2,$ where $v'_y 2$ and v_y^2, respectively, are the velocities of the particle after and before collision with the cell's wall. The cell is assumed to move with a velocity V_{dr}. The relative velocity equation gives $v' - V_{dr} = \alpha(V_{dr} - v)$, where α is the normal restitution coefficient between the particle and the wall. The change in kinetic energy of one particle may then be rewritten as $\Delta E(v_y, V_{dr}) = \frac{m}{2}[(1+\alpha)^2 V_{dr}^2 - 2(1+\alpha)V_{dr}v_y - v_y^2(1-\alpha 2)]$ and the energy flux j_{dr}, associated with particles going toward the wall, can be expressed as $j_{dr} = \frac{N_H}{2h_H} v_y \Delta E(v_y, V_{dr})$, where we have assumed that $N_H/2$ particles are going toward the wall. The net energy flux for a given wall velocity is then obtained by averaging the flux of the incoming particles with the velocity distribution function, $f(v_y)$ associated with the "cold" region and integrating on the velocities directed towards the wall:

$$J_{dr}(V_{dr}) = \int_0^\infty j_{dr} f(v_y) dv_y \tag{5}$$

where the distribution function of the velocity is the Gaussian one retrieved from experiments (**Figure 14**).

The integral (5) over the velocities gives the following result

$$J_{dr}(V_{dr}) = \frac{m}{4}\frac{N_H}{h_H}[(1+\alpha)^2 V_{dr}^2 I_1 - 2(1+\alpha)V_{dr}I_2 - (1-\alpha 2)I_3] \tag{6}$$

I_1, I_2, and I_3 are the integrals $\int_0^\infty v_y^i f(v_y)\, dv_y$ $(i = 1..3)$ which are, respectively, given by:

$$I_1 = \sqrt{\frac{T_y}{2\pi m}} I_2 = \frac{T_y}{2m} I_3 = \left(\frac{T_y}{m}\right)^{\frac{3}{2}} \sqrt{\frac{2}{\pi}} \tag{7}$$

We may assume that the particles go from the bulk towards the "hot" areas (double collisions are neglected) so that with the average velocity found experimentally and that we are using in the comparisons. The last thing to do is to compute the average on the wall velocity: the linear term in V_{dr} cancels while the term related to V_{dr}^2 averages to $(A\omega)2/2$. Multiplying by 2 (because of 2 moving walls) gives the following expression for the injected flux of energy:

$$J_{dr} = m\frac{N_H}{2h_H}\left[(1+\alpha)2(V_{dr})2\sqrt{\frac{T_y}{2\pi m}} - (1-\alpha 2)\left(\frac{T_y}{m}\right)^{\frac{3}{2}}\sqrt{\frac{2}{\pi}}\right] \tag{8}$$

For perfectly elastic walls ($\alpha = 1$), the expression proposed by Soto [35] for a sinusoidal vibration taking for their function $q\left(T/m(A\omega)2\right)$ is recovered; the constant $q = \sqrt{2/\pi} = 0.8$ is a very good approximation for our experimental conditions and our values of $T/m(A\omega)2$. The additional contribution to the energy input from g-jitter (even if it has quite no impact on the velocities of the free floating particles in microgravity) can create an additional contribution to

the wall velocity and so to the energy injected into the medium. This can be estimated as $\langle \delta V^2 = 0.005\ m^2/s^2 \rangle$ [41]. Since it does not exceed 15% of V_{dr}^2 in the worst case, it was neglected. The equilibrium between injection (Eq. (8)) and dissipation (Eq. (4)) gives:

$$T_y = \frac{\frac{N_H}{2h_H}(1+\alpha)2}{\frac{N_C^2}{h_C L_x}\ \pi\sigma g_2(\varphi)\frac{1-e2}{2}\left(1+\frac{1}{R_T}\right)^{3/2} + 2\frac{N_H}{h_H}(1-\alpha 2)} m(A\omega)2 \tag{9}$$

The temperature is proportional to the square of the amplitude of the driving velocity as it should have been shown in Ref. [13]. The densities in the "cold" and "hot" areas are known so that we can compare the predictions of Eq. (9) with our experimental values of T_y calculated. To consider the dissipation due to the tangential restitution coefficient β, we introduce an effective restitution coefficient r_e proposed by McNamara and Luding [41] instead of e in Eq. (9): $r_e = \sqrt{e^2 - \left(q(1-\beta^2)\right)/(1+2q-\beta)}$. Using $q = 0.5$ for a disk and $\beta = 0.7$;, we obtain $r_e = 0.462$ instead of $e = 0.64$. The comparison between the theoretical temperatures T_y obtained from Eq. (9) with the experimental ones calculated in the "cold" region is presented in **Figure 16**.

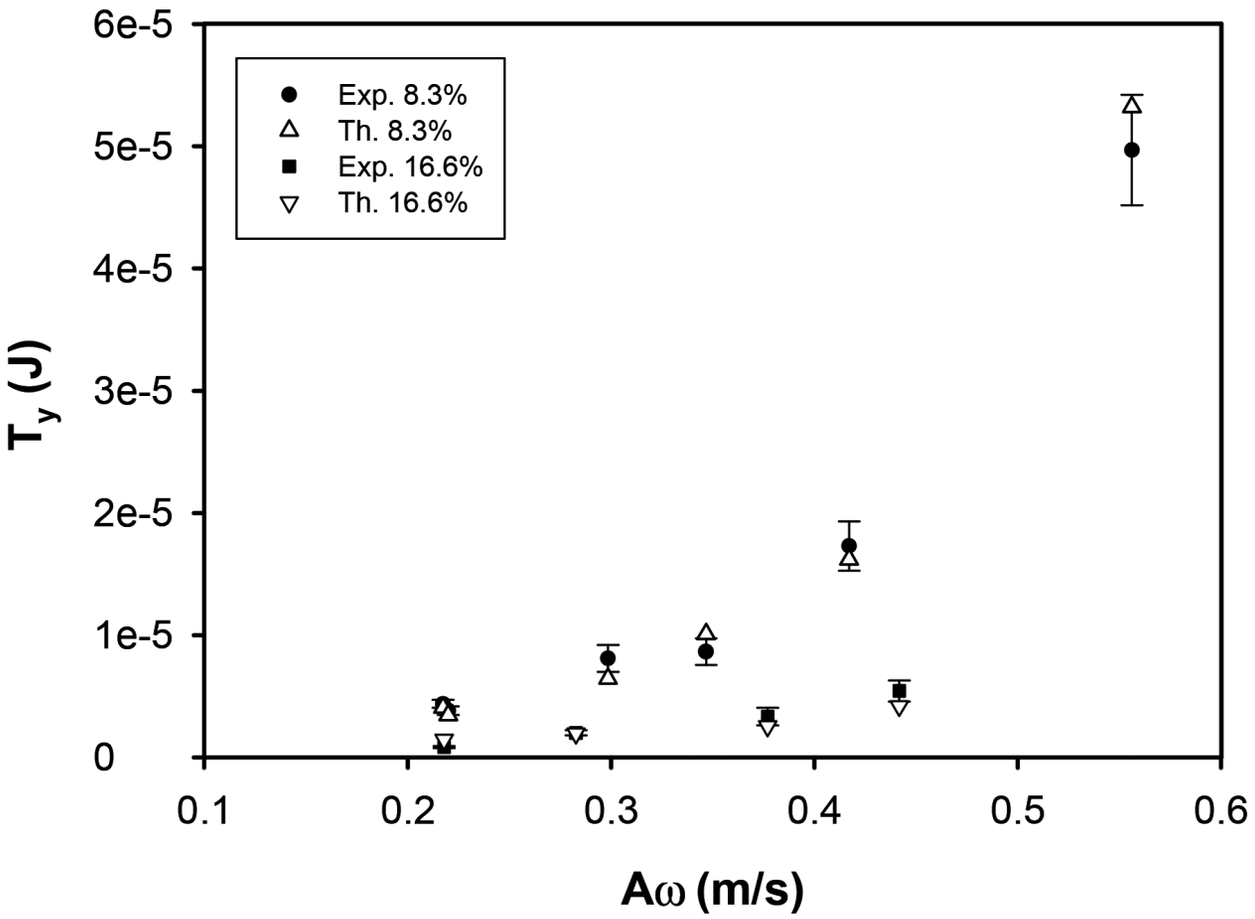

Figure 16. Comparison of the equilibrium temperature computed from Eq. (9) as a function of the driving velocity of the cell ($A\omega$).

With the two area fractions, we have used in this study, one can see that the agreement is good. Of course, to improve the theoretical prediction of the temperature with the driving velocity, being able to predict the density N_H/h_H close to the top and bottom walls instead of considering the experimental value obtained from the profiles.

The anisotropy found for the temperatures created by a vibrating wall is scarcely reviewed in the literature. A recent experiment with a setup including a 3D-cylindrical [42] where the anisotropic behavior of the ratio $R_T = T_y/T_x$ is reported as a function of the volume fraction of particles shows a strong increase for values below 10%, but it still remains smaller than our results. Moreover, a theoretical study including two different Maxwellian distributions for parallel and perpendicular directions about the vibration and a density along the vibration axis is presented in Ref. [43]. A balance between energy fluxes along the direction of vibration and perpendicular to it gives the ratio R_T and predicts that, for perfectly elastic walls, this ratio would only depend on the restitution coefficient. This is not our experimental situation where the ratio R_T is much larger for the lowest density. Thus, it impossible to relate this theoretical approach with our study since our density profile is much different for a one driven by gravity. Nevertheless, we may predict values of R_T if we assume a constant density in the "cold" area.

4. Conclusion

We have reported experimental investigations on the dynamics of a model granular medium. Experiments have been performed in a low-gravity environment. The cell containing the medium is subjected to external vibration which drives the collective motion of the particles. As the dynamical behavior of the medium is driven by the kinematics of the particles, high-speed video recording coupled to an individual particle tracking technique allows to obtain the trajectory of each particle. From these raw data, the inelastic parameters of the particles which are at the origin of the dynamics of the whole medium can be retrieved as well as a direct measurement of the energy (or temperatures). We have found that depending on the type of particles used, the normal restitution coefficient can be dependent on the relative impact velocity between two particles but not always. One way to characterize the inelastic nature of the collisions is to look to the energy decay once the medium is freely evolving. We have obtained smaller experimental relaxation times of this energy than the ones predicted by theories at least if we do not take into account the velocity dependent of this restitution coefficient. It is also interesting to note that the effect played by the rotation of the particles can significantly affect the whole behavior of the medium. In particular, we have reported the translational temperatures along and perpendicular to the direction of vibration as well as the rotational temperatures. When compared to existing theories, it appears that there are significant differences which also depend on the driving velocity and on the concentration of the medium. Two major points on the comparison can be raised: First the density is not homogeneous in the cell and second the translational velocities are much higher in the direction of vibration than perpendicular to it (versus a homogeneous input of energy as considered in theories). We report that the balance of the energy fluxes along the vibration can correctly represent the behavior of the granular temperature with the driving velocity of the cell and

with the area fraction. In this balance, the contribution of the tangential velocities to the dissipation must be considered. At least the distinction between the dissipation due to the collisions between the particles which is proportional to the average temperature $T = (T_x + T_y)/2$ and the driving flux, which depends only on T_y, was introduced, but on the basis of the experimental ratio T_y/T_x. This ratio increases when the volume fraction decreases and it also depends on the driving velocity. A theoretical determination of T_y/T_y which could reproduce these behaviors should involve the non-elastic collisions with the lateral walls, but is let for a future developments.

Acknowledgements

The authors like to thank NOVESPACE and the CNES for giving them the possibility to board the A300-zero G in order to perform the experimental study.

Author details

Yan Grasselli[2]*, Georges Bossis[1], Alain Meunier[1] and Olga Volkova[1]

*Address all correspondence to: yan.grasselli@skema.edu

1 Laboratoire de la Matière Condensée, University of Nice Sophia Antipolis, Parc Valrose, France

2 SKEMA Business School, University of Côte d'Azur, Sophia-Antipolis, France

References

[1] Pöschel T, Luding S, editors. Granular Gases. Springer; Berlin, 2001

[2] Pöschel T, Brilliantov NV, editors. Granular Gas Dynamics. Springer; Berlin, 2003

[3] Barrat A, Trizac E, Ernst MH. Granular gases: Dynamics and collective effects. Journal of Physics: Condensed Matter. 2005;**17**:S2429

[4] Aranson IS, Tsimring LS. Patterns and collective behavior in granular media: Theoretical concepts. Reviews of Modern Physics. 2006;**78**:641

[5] Puglisi A, editor. Transport and Fluctuations in Granular Fluids: From Boltzmann Equation to Hydrodynamics Diffusion and Motor Effects. Springer; Berlin, 2014

[6] Kudrolli A, Wolpert M, Gollub JP. Cluster formation due to collisions in granular material. Physical Review Letters. 1997;**78**:1383

[7] Opsomer E, Ludewig F, Vandewalle N. Phase transitions in vibrated granular systems in microgravity. Physical Review E. 2011;**84**:051306

[8] Falcon E, Wunenburger R, Evesque P, Fauve S, Chabot C, Garrabos Y, Beysens D. Cluster formation in a granular medium fluidized by vibrations in low gravity. Physical Review Letters. 1999;**83**:440

[9] Falcon E, Aumaıtre S, Evesque P, Palencia F, Lecoutre-Chabot C, Fauve S, Beysens D, Garrabos Y. Collision statistics in a dilute granular gas fluidized by vibrations in low gravity. Europhysics Letters. 2006;**74**:830

[10] Noirhomme M, Opsomer E, Vandewalle N, Ludewig F. Granular transport in driven granular gas. The European Physical Journal E. 2015;**38**:9

[11] Opsomer E, Noirhomme M, Vandewalle N, Falcon E, Merminod S. Segregation and pattern formation in dilute granular media under microgravity conditions. Nature. Article number: 1, 2017;**3**

[12] Bossis G, Grasselli Y, Volkova O. Granular rheology in zero gravity. Journal of Physics: Condensed Matter. 2004;**16**:3279

[13] Bhateja A, Sharma I, Singh JK. Scaling of granular temperature in vibro-fluidized grains. Physics of Fluids. 2016;**28**:043301

[14] Pathak SN, Jabeen Z, Das D, Rajesh R. Energy decay in three-dimensional freely cooling granular gas. Physical Review Letters. 2014;**112**:038001

[15] Huthmann M, Aspelmeier T, Zippelius A. Granular cooling of hard needles. Physical Review E. 1999;**60**:654

[16] Villemot F, Talbot J. Homogeneous cooling of hard ellipsoids. Granular Matter. 2012;**14**:91

[17] Harth K, Kornek U, Trittel T, Strachauer U, Home S, Will K, Stannarius R. Granular gases of rod-shaped grains in microgravity. Physical Review Letters. 2013;**110**:144102

[18] Yan-Pei C, Evesque P, Mei-Ying Chin H. Breakdown of energy equipartition in vibro-fluidized granular media in micro-gravity. Physics Letters. 2012;**29**:074501

[19] Brilliantov NV, Pöschel. Kinetic Theory of Granular Gases. Oxford University Press; 2004

[20] Tatsumi S, Murayma Y, Hayakawa H, Sano M. Experimental study on the kinetics of granular gases under microgravity. Journal of Fluid Mechanics. 2009;**641**:521

[21] Grasselli Y, Bossis G. Three-dimensional particle tracking for the characterization of micrometer-size colloidal particles. Journal of Colloid and Interface Science. 1995;**1**:269

[22] Gondret P, Lance M, Petit L. Bouncing motion of spherical particles in fluids. Physics of Fluids. 2002;**14**:268

[23] KantakAdvait Ashok. Wet particles collisions [thesis]. University of Colorado at Boulder: 2005. DOI: AAT 3190381

[24] Sorace CM, Louge MY, Crozier MD, Law VHC. High apparent adhesion energy in the breakdown of normal restitution for binary impacts of small spheres at low speed. Mechanics Research Communications. 2009;**36**:364

[25] Chapman S, Cowling TG, editors. The Mathematical Theory of Nonuniform Gases. London: Cambridge University Press; 1960

[26] Miller S, Luding S. Cluster growth in two-and three-dimensional granular gases. Physical Review E. 2004;**69**:031305

[27] Hou M, Liu R, Zhai G, Sun Z, Lu K, Garrabos Y, Evesque P. Velocity distribution of vibration-driven granular gas in Knudsen regime in microgravity. Microgravity Science and Technology. 2008;**20**:73

[28] Tatsumi S, Murayama Y, Sano M. Experimental Study of the Freely Evolving Granular Gas under Microgravity Condition. AIP Conference Proceedings. 2008;**1027**:923

[29] Maaß C, Isert N, Maret G, Aegerter CM. Experimental investigation of the freely cooling granular gas. Physical Reviews Letters. 2008;**100**:248001

[30] Chen Y, Hou M, Evesque P, Jiang Y, Liu M. Asymmetric velocity distribution in boundary-heating granular gas and a hydrodynamic description. Powders & Grains. 2013;**1542**:791

[31] Labous L, Rosato AD, Dave RN. Measurements of collisional properties of spheres using high-speed video analysis. Physical Review E. 1997;**56**:5717

[32] Grasselli Y, Bossis G, Goutallier G. Velocity-dependent restitution coefficient and granular cooling in microgravity. European Physical Letters. 2009;**86**:60007

[33] Das S, Puri S. Pattern formation in the inhomogeneous cooling state of granular fluids. Europhysics Letters. 2003;**61**:749

[34] Evesque P. Powders & Grains. 2001;**12**:60

[35] Soto R. Granular systems on a vibrating wall: The kinetic boundary condition. Physical Reviews E. 2004;**69**:061305

[36] Rivas N, Luding S, Thornton AR. Low-frequency oscillations in narrow vibrated granular systems. New Journal of Physics. 2013;**15**:113043

[37] Jenkins T, Zhang C. Kinetic theory for identical, frictional, nearly elastic spheres. Physics of Fluids. 2002;**14**:1228

[38] Herbst O, Cafiero R, Zippelius A, Herrmann HJ, Luding S. A driven two-dimensional granular gas with Coulomb friction. Physics of Fluids. 2005;**17**:107102

[39] Falcon E, Bacri J-C, Laroche C. Equation of state of a granular gas homogeneously driven by particle rotations. Powders & Grains. 2013;**1542**:815

[40] vanNoije TPC, Ernst MH. Velocity distributions in homogeneous granular fluids: The free and the heated case. Granular Matter. 1998;**1**:57

[41] McNamara S, Luding S. Energy flows in vibrated granular media. Physical Review E. 1998;**58**:813

[42] Windows-Yule CRK, Parker DJ. Boltzmann statistics in a three-dimensional vibrofluidized granular bed: Idealizing the experimental system. Physical Review E. 2013;**87**:022211

[43] van der Meer D, Reimann P. Temperature anisotropy in a driven granular gas. Europhysics Letters. 2006;**74**:384